Orbital contributions to the magnetic susceptibility of one-dimensional Hubbard models with partial filling and strong correlation

S. A. Bewick and Z. G. Soos
Department of Chemistry, Princeton University, Princeton, New Jersey 08544, USA
(Received 28 February 2006; revised manuscript received 5 October 2006; published 30 November 2006)

The one-dimensional (1D) Hubbard model with partial filling $\rho<1$ and strong correlation $U>4t$ is approximated by a t-J model with real transfers t between adjacent occupied and empty sites, and virtual transfers J between adjacent spin-paired sites. Finite t-J models with $\rho<1$ preserve spin-charge separation in the atomic limit ($J=0$) for open boundary conditions, but not for periodic boundary conditions. The absolute magnetic susceptibility $\chi(T)$ of finite systems is found exactly and shown to converge to the infinite chain when k_BT exceeds J. Strong orbital contributions to $\chi(T)$ are demonstrated in systems with t, J, and ρ chosen to have identical $\chi(0)$ per electron, as known exactly for the 1D Hubbard model. Orbital contributions for $\rho<1$ preclude treating the spin susceptibility of partly filled bands in terms of $\rho=1$ systems such as Heisenberg spin chains, as assumed previously. Orbital contributions at $\rho=0.6$ are used to model the spin susceptibility of tetrathiafulvalene-tetracyanoquinodimethan above the metal-insulator transition, both at constant spacing along the stack and with a linear $t(T)$. The parameters at $T\sim100$ K are $t=0.15$ eV and $J=2t^2/U=0.053$ eV, indicative of strong correlation $U>4t$ in this prototypical organic salt.

DOI: 10.1103/PhysRevB.74.205125 PACS number(s): 71.10.Fd, 75.30.Cr, 71.28.+d, 71.20.Rv

I. INTRODUCTION

The organic conductor TTF-TCNQ (tetrathiafulvalene-tetracyanoquinodimethan) has parallel segregated stacks of donors with $\rho=0.59$ holes per TTF and acceptors with $\rho=0.59$ electrons per TCNQ. The physical properties of TTF-TCNQ single crystals have been intensively studied[1,2] in connection with its high metallic conductivity, its metal-insulator transition at 54 K, and phase transitions at lower temperature associated with TTF or TCNQ stacks. Electrical conductivity has primarily been modeled in terms of one-dimensional (1D) bands with electron-phonon coupling leading to a Peierls transition at 54 K. The electronic structure of either stack can be approximated by a 1D Hubbard model with on-site repulsion $U>0$ and density $\rho=0.59$. The relative magnitude of U and $4t$, the width of the 1D band, describes electron-electron correlation, with $U=0$ for free electrons, $U<4t$ for weak correlation and $U>4t$ for strong correlation. Although TTF-TCNQ data taken separately could often be treated in impressive detail, a consistent overall model of electrical, optical, magnetic, and structural properties has not been reached.

Torrance *et al.*[3] championed the minority view of $U>4t$, based initially on the molar magnetic susceptibility $\chi(T)$ of TTF-TCNQ shown in Fig. 1, and on neutron scattering data. They noted that the *magnitude* of $\chi(350\ \mathrm{K})$ could be fit to a 1D band with $U=0$, to a band with Stoner enhancement for $U<4t$, or to a spin-1/2 Heisenberg antiferromagnetic (HAF) chain with $J=200$ K for $U>4t$. The HAF curve in Fig. 1 has $J=360$ K and matches experiment at the transition. Since none of these models accounts for the temperature dependence of $\chi(T)$ for $T>54$ K, Torrance *et al.*[3] could only advance qualitative arguments for $U>4t$ in TTF-TCNQ. Closely similar $\chi(T)$ data were reported by others.[4] Klotz *et al.*[5] subsequently measured $\chi(T)$ under pressure up to 10 kbar in order to extract the susceptibility at constant spacing along the stack. The pressure dependence suggested large U, but the analysis remained qualitative. We present in this paper $\chi(T)$ calculations for partly filled bands with $U>4t$ by exact treatment of oligomers and demonstrate that, contrary to previous expectations, $\chi(T)$ for $\rho<1$ cannot be represented by a HAF chain with an effective J.

The t-J model[6] is associated with partly filled bands in high-T_c superconductors. It describes real and virtual electron transfer between neighbors in lattices such as square-planar copper oxide layers. The t-J model in 1D is

$$H(t,J) = -t\sum_{p\sigma} P(a^{+}_{p\sigma}a_{p+1\sigma} + \mathrm{h.c.})P + 2J\sum_{p}(\vec{s}_p\cdot\vec{s}_{p+1} - n_pn_{p+1}/4), \quad (1)$$

where P is the projector that excludes $n_p=2$ fermions at any site, either two electrons at a TCNQ site or two holes at a TTF site. The first term gives a tight-binding band of spinless fermions whose remarkable properties have been discussed by Lieb and Mattis[7] and by Brinkman and Rice.[8] These fer-

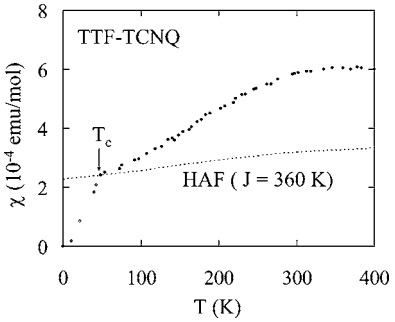

FIG. 1. Temperature dependence of the molar susceptibility of TTF-TCNQ. The data are from Ref. 3 and include diamagnetic corrections. The HAF curve is for a spin chain with exchange $J=360$ K.

mions govern the charge degrees of freedom. The second term describes virtual transfers J at neighboring sites with $n_p=1$. The $J=0$ limit corresponds to the atomic limit of the Hubbard model and illustrates spin-charge separation. Klein and Seitz[9] obtained an effective Hamiltonian for small J that coincides with (1) by projecting the Hubbard model onto the subspace with $n_p=0$ or 1. They were perhaps the first to study the t-J model under another name. Near the atomic limit, the relation $2t/U=J/t$ connects the Hubbard and t-J models, with $U=4t$ at $J=t/2$.

Among exact results for the 1D Hubbard model at $T=0$, Shiba[10] obtained $\chi(0)$ per electron for arbitrary density $\rho \leqslant 1$ and correlation U/t. To leading order in $t/U<1$, $\chi(0,\rho)$ is inversely proportional to the AF exchange constant $J(\rho)$ given by[10]

$$J(\rho) = J\rho(1 - \sin 2\pi\rho/2\pi\rho), \tag{2}$$

with $J=2t^2/U$. Since the effective Hamiltonian of Klein and Seitz[9] leads to the same $J(\rho)$, it has been generally assumed that $\chi(T)$ of partly filled Hubbard models remains of the HAF form. This is not the case, however. Correlated systems with *identical* $J(\rho)$ and hence $\chi(0,\rho)$ will be shown to differ substantially at $k_BT \sim J(\rho)$ due to charge degrees of freedom in partly filled bands. Our results are restricted to systems with negligible thermal population of doubly occupied sites, or $k_BT \ll U$, which follows from $k_BT \sim J(\rho)$ and $U>4t$.

Many theoretical approaches have been applied to infinite 1D Hubbard, Heisenberg, or t-J models, including exact results at $T=0$, variational functions for the ground state (GS), and a variety of approximations including density matrix renormalization group (DMRG) methods. Sirker and Klumper[11] have recently summarized results for the 1D t-J model with $J'=2J$ in (1). Variational methods[12–14] and numerical extrapolations[15] have focused on GS properties and the 0 K phase diagram. The Bethe ansatz yields exact results at the supersymmetric point, $t=J$, and there is phase separation at even larger J. Takahashi's early proposal,[16] a thermal Bethe ansatz (TBA) for the 1D Hubbard model, has generated much theoretical interest, again motivated by high T_c, first in connection with the string hypothesis[17] and the validity[18] of TBA. TBA generates an infinite set of integral equation whose approximate solution[19] requires truncation. Another approach to the thermodynamics was taken by Jüttner *et al.*,[20] who mapped the 1D Hubbard model to the 2D Shastry model and reduced the problem to a finite number of coupled nonlinear integral equations. Their quantum transfer matrix (QTM) approach resembles DMRG in becoming highly accurate as the Trotter number M is increased. Quantum Monte Carlo is yet another general approach[21] to the thermodynamics of the 1D Hubbard model. In these works,[17,19–21] $\chi(T,\rho)$ in systems with $U>4t$ has been of secondary interest with brief comments in support of HAF behavior that we argue against for $\rho<1$. Since our $\chi(T,\rho)$ curves at $U=8t$ agree well with Refs. 20 and 19, orbital contributions could have been previously inferred.

The physical regime relevant to TTF-TCNQ or organic conductors has $U>2t$, or $J<t$. Bonner and Fisher[22] obtained $\chi(T)$ of HAF chains using direct solution of finite chains with $N<12$ spins. We have recently extended $\chi(T)$ to $N=18$ spins in order to model a spin-Peierls transition.[23] Johnston *et al.*[24] have comprehensively discussed theoretical results for the HAF, the special case of (1) with $\rho=1$. Thermodynamic quantities converge rapidly with N when there is substantial population in excited states, but are limited by finite-size gaps at low T. The exact[10] $\chi(0,\rho)$ is consequently essential for our analysis.

In this paper, we apply $H(t,J)$ in (1) to partly filled bands with strong correlations using the real-space basis of valence bond (VB) diagrams.[25] The t-J model approximates a Hubbard model with $U>4t$, but is computationally less demanding because $n_p=2$ sites are excluded. The restriction to finite systems has implications for the atomic limit, as shown in Sec. II. Spin-charge separation fails for periodic boundary conditions (PBC), but is preserved for open boundary conditions (OBC). Sec. III presents the spin susceptibility as a function of J/t, band filling, and size. The TTF-TCNQ susceptibility at $T \sim 100$ K and constant spacing along the stack is modeled with $t=0.15$ eV and $J/t=0.35$, in the range suggested by Torrance *et al.*[3] Thermal expansion is included via a linear $t(T)$ dependence to model $\chi(T)$ at ambient pressure. We discuss in Sec. IV the origin of orbital contributions to $\chi(T)$.

II. ATOMIC LIMIT OF FINITE 1D HUBBARD MODELS

We consider $H(t,0)$ with real transfers t in (1) and $J=0$ in the atomic limit ($U/t \to \infty$). There are $N_e=2R$ electrons or holes on N sites at the density $\rho=2R/N \leqslant 1$. The number of ways to distribute $2R$ charges on N sites gives the *orbital* degrees of freedom,

$$W(2R,N) = \frac{N!}{(2R)!(N-2R)!}. \tag{3}$$

Each orbital state has *spin* degeneracy of 2^{2R}. Spin-charge separation has long been recognized at $\rho=1$, where $W(N,N)=1$ and a linear HAF describes the spin excitations of the Hubbard model, and in extended 1D systems with $\rho<1$, where Lieb and Mattis[7] showed that the ground state (GS) is a singlet for any spin-independent interaction between electrons. Spin-charge separation is retained in the atomic limit of finite Hubbard models with open boundary conditions (OBC), but not with periodic boundary conditions (PBC). This has the important consequence of requiring OBC for our primary goal of using finite systems to model extended chains.

We summarize OBC results before turning to PBC. In the ferromagnetic (FM) subspace with parallel spins and $S=R$, the constraint $n_p<2$ is enforced by the Pauli exclusion principle, independently of electron-electron interactions. We have a Hückel chain for spinless fermions with single-particle energies, in units of $t=1$,

$$\varepsilon(r,N) = -2\cos(\pi r/(N+1)), \quad r = 1,2,\ldots,N. \tag{4}$$

The corresponding normalized eigenfunctions are linear combinations of site functions

$$|r\rangle = \sum_p c_{pr}|p\rangle, \quad c_{pr} = \sqrt{2/(N+1)}\,\sin[\pi pr/(N+1)]. \quad (5)$$

The band is filled to $r=2R$ in the GS of the FM subspace. The charge density at site p is

$$\rho_p = \sum_{r,filled} c_{pr}^2. \quad (6)$$

Alternate symmetry relates the orbital r to the orbital $r'=\mathrm{N}+1-r$ with $\varepsilon_{r'}=-\varepsilon_{\mathrm{r}}$ and ${c_{pr'}}^2={c_{pr}}^2$ at all sites p. The quarter-filled chain consequently has uniform $\rho_p=1/2$.

In subspaces with $S<R$, the exclusion of $n_p=2$ is enforced by $U/t\to\infty$. We use OBC to take advantage of the fact that it is then possible to order[7] fermions in 1D. If $2R$ fermions are placed on a lattice such that $p_1<p_2<\cdots p_{2R}$, the order is preserved under nearest-neighbor electron transfer when $n_p=2$ sites are excluded. For each choice of occupied sites, we construct eigenstates of S by forming linear combinations of sites with spin α and β. The number of representation of a given S, each with $2S+1$ values of S_z, is[26]

$$N(S,2R) = \frac{(2S+1)(2R)!}{(R-S)!(R+S+1)!}, \quad S=0,1,\ldots,R. \quad (7)$$

Valence bond (VB) diagrams $|\mathrm{k}\rangle$ are many-electron functions in real space with fixed S.[25] Since OBC preserves the order $p_1<p_2<\cdots p_{2R}$, the connectivity of VB diagrams is also conserved. It follows that each $N(S,2R)$ representation of total S in (7) leads to an identical matrix $H(t,0)$, and that $H(t,0)$ is the same for all S. The single-particle energies $\varepsilon(r,N)$ in (4) lead to $2R$-fermion states on filling $2R$ different levels. Precisely the same $2R$-fermion energies and charge distributions are found for any S in the limit $U/t\to\infty$. The OBC result is general, since the matrix representation of $H(t,0)$ in the VB basis is straightforward for any N and $2R=N_e$.

For PBC, the single-particle energies in the FM subspace are

$$\varepsilon(k,N) = -2\cos k. \quad (8)$$

Translational symmetry leads as usual to wave vectors $\mathbf{k}$ in the first Brillouin zone,

$$\mathbf{k} = 0, \pm 2\pi/N, \pm 4\pi/N, \ldots, \pi \quad (9)$$

for even N. The GS for $2R$ spinless fermions is immediately seen to be twofold degenerate, with $k_{\mathrm{F}}=\pm\pi\rho$, in contrast to the nondegenerate GS under OBC. Transfer between sites 1 and N spoils the ordering of fermions. As a consequence, VB diagrams with $S<R$ and different pairing patterns are mixed in the atomic limit, and the eigenvalues of $H(t,0)$ depend on S in finite PBC systems.

Subspaces with $S<R$ have one or more reversed spins. The following analysis came out of direct VB solution of finite PBC systems that were originally run to check programs for partly filled bands. $2R$-fermion states with $S<R$ have expanded unit cells of $2RN$ in real space. We introduce a common phase factor α for all fermions

TABLE I. Values of $N\alpha/\pi$ in Eq. (10) found by solving $H(t,0)$ with periodic boundary conditions for $2R=4$ or 6 electrons on $N=6$, 8, 10, or 12 sites. The degeneracy of each α is given in parenthesis.

S	$4/N$	$6/N$
0	0, 2	0, ±1, 3(2)
1	±1, 2	0(2), ±1, ±2(2),
2	0	±1, ±2, 3
3	—	0

$$\alpha = 0, \pm\pi/NR, \ldots, \pi/N. \quad (10)$$

The $2R$ values of α give a wave vector $\mathbf{k}$ when multiplied by $2R=N_e$. The angular momentum problem is to construct eigenstates of S and S_z. The function $|2R,2R-1\rangle$ has $S_z=2R-1$ and $\alpha=0$. The $2R-1$ functions with $S=S_z=2R-1$ have the remaining values of α and single-particle energies $-2\cos(\mathbf{k}-|\alpha|)$ in (8). The GS energy per site of $2R$ fermions depends on α, and hence on S,

$$\varepsilon_0(\rho,N,\alpha) = -\frac{2}{N}\sum_{k=R-1}^{R}\cos\left(\frac{2\pi k}{N}-|\alpha|\right) = -\frac{2\sin(\pi\rho)\cos(\pi/N-|\alpha|)}{N\sin(\pi/N)}. \quad (11)$$

The band limit of $-2\sin(\pi\rho)/\pi$ is recovered for spinless fermions, independently of α, and the extended system has spin-charge separation, but its wave functions are not accessible. The $S<R$ eigenstates are correlated $2R$-electron functions in terms of translational symmetry that nevertheless have a single-particle spectrum on including the phase α.

The minimum of ε_0 is at $\alpha=\pi/N$ for finite N and $\rho<1$; the $2R$-fermion GS is nondegenerate with total $\mathbf{k}=0$. The GS with $\alpha=0$ has higher energy by $\pi\sin(\pi\rho)/N$. In agreement with the Lieb-Mattis theorem,[7] the absolute GS is a nondegenerate singlet for all the $2R,N$ combinations that we solved directly. Finite PBC systems have $W(2R,N)$ orbital excitations, as expected. The unexpected result was that all $W(2R,N)$ excitations are quantitatively related to the single-particle energies, $-2\cos(\mathbf{k}-|\alpha|)$, in which each of the $N(S,2R)$ representations in (7) has one of the phases α in (10). We did not know in general how many times a given α appears for each S, aside from the $S=R$ and $R-1$ cases. The atomic limit still reduces to free spinless fermions, as recognized[7–9] in extended systems, but the single-particle energies of finite PBC systems with $\rho<1$ have a residual dependence on S. There is no spin-charge separation in the atomic limit of finite PBC systems. We have solved finite systems whose orbital degeneracy $W(2R,N)$ and number of representations $N(S,2R)$ are each $\sim$100. Table I lists values of α in four- and six-electron systems with variable even N up to 12. The single-particle energies of $2R$-fermion states depend on S through α in (10), with the 2^{2R} spin states with the lowest orbital energy distributed over the $R+1$ values of $\varepsilon_0(\rho,N,\alpha)$ in (11). The S dependence of α is entirely due to

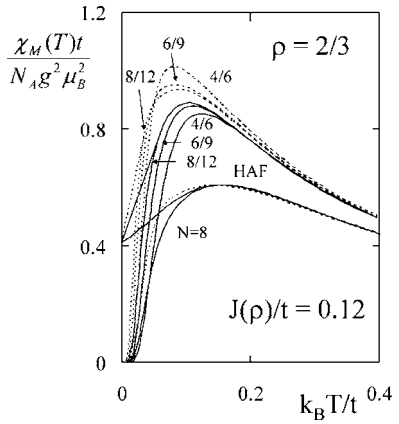

FIG. 2. Spin susceptibility per electron of t-J oligomers at density $\rho=2/3$ with open boundary conditions for t in Eq. (1). Solid and dashed lines have periodic and open boundary conditions for small $J/t=0.15$ $(U/t=40/3)$. The open circle is the exact $\chi(0)$ of the infinite chain, from Ref. 10. The HAF curves are for the infinite chain with J in Eq. (2) adjusted to give the same $\chi(0)$. The $N=8$ spin chains with periodic and open boundary conditions illustrate size convergence.

electron transfer between sites 1 and N. Since we are interested in extended t-J models, we use OBC for real transfers in (1) from now on.

III. SPIN SUSCEPTIBILITY OF THE T-J MODEL

Virtual transfers J in (1) do not change the charge or spin degrees of freedom. The eigenvalue problem for $H(t,J)$ involves a series of matrices whose dimensions are $W(2R,N)N(S,2R)$ for $S=0,1,\ldots,\mathrm{R}$. To minimize end effects, we use both PBC and OBC for virtual transfers, but only OBC for real transfers. Reflection symmetry about the center reduces the dimensions by about a factor of 2. Matrices up to 8,000 suffice for the finite systems discussed below. All thermodynamic quantities are obtained from the partition function,

$$Q(R,N,\beta)=\sum_{S=0}^{R}\sum_{r=1}(2S+1)\exp(-\beta E_{Sr}), \qquad (12)$$

where $\beta=1/k_{\mathrm{B}}T$ and E_{Sr} is the excitation energy from the singlet GS to the rth state with spin S. The absolute susceptibility per mole of electrons or holes is

$$\chi_M(\rho,N,\beta)=\frac{N_{\mathrm{A}}\beta g^2\mu_{\mathrm{B}}^2}{3\rho NQ}\sum_{S=1}^{R}S(S+1)(2S+1)\sum_{r=1}\exp(-\beta E_{Sr}), \qquad (13)$$

where N_{A} is Avogadro's number, μ_{B} is the Bohr magneton, and the g value of organic radicals is close to 2.00236, the free-electron value.

The convergence of $\chi(T)$ with N has been studied in detail for HAF chains with $\rho=1$. Figure 2 presents similar $\chi(T)$ results as a function of $k_{\mathrm{B}}T/t$ for density $\rho=2/3$ and small $J/t=0.15$ close to the atomic limit $(U/t=40/3)$, where finite

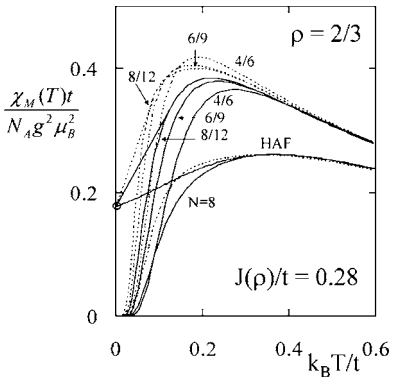

FIG. 3. Same as Fig. 2 for larger $J/t=0.35$ that gives to $U/t\sim 5.7$.

t/U and $J=2t^2/U$ in (2) give a 2.7% correction to $\chi(0)$ at $\rho=1$. To conserve total exchange we take J for PBC (shown as solid lines) and $J'=JN/(N-1)$ for OBC (shown as dashed lines). Good convergence is found even in small systems for T above the $\chi(T)$ peak. Near the peak the OBC and PBC curves converge from above and below respectively to an accuracy of about 5%. The exact[10] $\chi(0)$ of the infinite Hubbard model with $J(2/3)/t=0.12$ in (2) is shown as an open circle. The HAF results in Fig. 2 are chosen to match at $T=0$, as shown for the extended chain and to illustrate convergence for eight spins with PBC or OBC at and above the $\chi(T)$ peak. The temperature dependence of $\chi(T)$ is clearly greater at $\rho=2/3$ than at $\rho=1$. The susceptibilities become equal for $k_{\mathrm{B}}T\gg J(\rho)$, merging as $C/[T+\theta(\rho)]$; the Curie constant $C=N_{\mathrm{A}}g^2{\mu_{\mathrm{B}}}^2/4k_{\mathrm{B}}$ is the same for an equal number of spins, while the Weiss constant $\theta(\rho)$ is related to J.

We note that while $\chi(0,\rho)$ is exact to leading order in t/U, linear interpolation to $\chi(0,\rho)$ is convenient but not correct. For the HAF chain, the slope of $\mathrm{d}\chi(T)/dT$ diverges[27] at $T=0$ and $\chi(T)$ is about 10% higher[27] at low $T<J/10k_{\mathrm{B}}$ than the linear interpolation of Bonner and Fisher.[22] The 1D Hubbard model has a similar increase of about 10% between $\chi(0,\rho)$ at $U=8t$ and $0.5\leqslant\rho\leqslant 1$ in Fig. 2 of Ref. 10 and the lowest $T>0$ points in Fig. 6 of Ref. 20. The $T\sim 0$ regime is of theoretical interest for Heisenberg, Hubbard, or t-J models, but is not accessible in TTF-TCNQ due to the metal-insulator transition with larger unit cell and sharply reduced $\chi(T)$ below $T_{\mathrm{c}}=54$ K.

Larger $J/t=0.35$ $(U/t\sim 5.7)$ is shown in Fig. 3 for $\rho=2/3$, again with both PBC and OBC for virtual transfers and with $\chi(0)$ fixed by $J(\rho)$. Increasing J reduces $\chi(T)$ as expected and shifts the maximum to higher T. Finite t/U now gives a 13% correction to $\chi(0,1)$ and the connection to t/J and Hubbard models is approximate, since $n_p=2$ sites are not excluded entirely at $U/t\sim 5.7$. The trends seen in Fig. 2 persist for increased exchange, both in terms of convergence and of orbital enhancement.

The ρ dependence of $\chi(T)$ versus $k_{\mathrm{B}}T/t$ is shown in Fig. 4 for six electrons on $6\leqslant N\leqslant 12$ sites and PBC for virtual transfers. Equal $\chi(0,\rho)$ follows on choosing J to give equal $J(\rho)$ in (2). Hence J doubles between $\rho=1$ and $\rho=1/2$. Similar results, not shown, are found at larger $J<t/2$. We did not

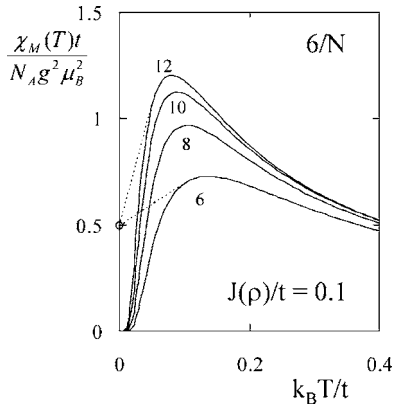

FIG. 4. Spin susceptibility per electron for six electrons on N sites and periodic boundary conditions for t (J) in Eq. (1). The choice of $J(\rho)$ in Eq. (2) yields identical $\chi(0)$ in infinite chains, shown as the open circle. Dashed lines are linear interpolations.

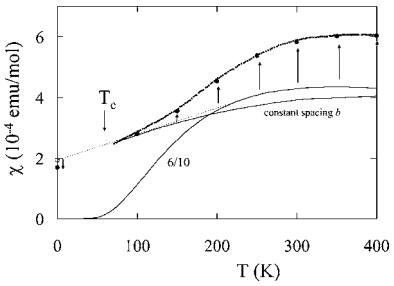

FIG. 5. Molar spin susceptibility, Eq. (13), of six electrons on ten sites with $t=0.15$ eV and $J/t=0.35$ in Eq. (1). The dashed line is a linear interpolation to $\chi(0)$, shown by the open circle. The data and constant b curve are from Ref. 5. Circles at 50 K intervals are calculated with linear $t(T)$ that decreases by 7% per 100 K increase, as discussed in the text.

pursue the weak dependence on J/t. The $6/N$ curves also merge as $C/[T+\theta(\rho)]$ at high temperature.

Figures 2–4 show deviations from HAF behavior with decreasing density that we attribute to orbital contributions. Previous studies at $U>4t$ found Heisenberg-like susceptibilities. The quantum Monte Carlo study of Hirsch and Scalapino[21] took $U=4t$, $\rho=1/2$, and focused on $2k_F$, $4k_F$ instabilities. The $\chi(T)$ results in Fig. 4(b) of Ref. 21 were fit near the peak to an HAF with an effective J given by (2), after noting scatter in the data and additional approximations at $T=0$. An HAF approximation to the $\rho=1/2$ curve in Fig. 4 would be about 20% too high at $T=0$ and 20% too low around the peak. Such a fit was reasonable at the time and consistent with expected HAF behavior. The thermal Bethe ansatz (TBA) study of Ha[17] focused on the string hypothesis and on high-T expansions of various quantities at $U=8t$, including $\chi(T,\rho)$ per site curves in Fig. 4(a) of Ref. 17. The peak region is poorly approximated, as seen by comparing $\rho=1$ to the HAF. Usuki *et al.*[19] present improved TBA results for $\chi(T,\rho)$ per site at $U=8t$ and $12t$ in Figs. 1(b) and 1(c) of Ref. 19 that are within a few percent of the QTM results of Jüttner *et al.* at $U=8t$ and $0.5\leqslant\rho\leqslant1$ in Figs. 5 and 6 of Ref. 20. We performed $N=10$ calculations at $U=8t$ and $12t$ for the same densities. The $\chi(T,\rho)$ peaks have similar positions and their magnitudes are about 10% above QTM, the most accurate method. Since the $N=8$ HAF maximum at $U/t\rightarrow\infty$ and constant $J=2t^2/U$ is almost quantitative in Fig. 2, the 10% difference between t-J and Hubbard models around the peak probably reflects finite U/t more than finite N. The orbital enhancement per spin shown in Fig. 4 down to $\rho=1/2$ is 15% greater than that inferred from Fig. 6 of Ref. 20.

The $\chi(T)$ data for TTF-TCNQ in Fig. 5 are from Klotz *et al.*,[5] who note that the absence of a maximum below 400 K is the only difference between their measurement and that of Torrance *et al.*[3] in Fig. 1. The estimated (smoothed) susceptibility at constant spacing b along the stack is from Fig. 5 of Ref. 5. Constant b is the best available approximation to constant volume[5] and hence to constant parameters. The calculated curve in Fig. 5 is based on (13) for six electrons or holes on ten sites with $t=0.15$ eV, $J/t=0.35$, and $g=2.0023$. The linear interpolation shown by a dashed line is to $\chi(0)$ for the extended system with $J(0.6)$ in (2). The fit is approximate but fairly demanding, since an absolute molar quantity is found. We have not sought the best fit for constant b, where pressure corrections are roughly approximated,[5] in order to treat accurate $\chi(T)$ data at ambient pressure. Constant b then refers to $T\sim100$ K at 1 atm.

The crystal structure of TTF-TCNQ at different temperatures[28] gives quantitative information about thermal expansion and $b(T)$, but leaves open the variation of $t(T)$. A linear dependence is a typical first approximation. Based primarily on TTF-TCNQ conductivity data, Conwell[29] estimated a change in t of (10 ± 5)% over a 200 K interval from 100 to 300 K. We take a 7% change in t per 100 K and note that $J/t=2t/U$ also changes by 7% per 100 K at constant U. The resulting $\chi(T)$, calculated at 50 K intervals, is shown in Fig. 5 by circles with arrows. They match the measured susceptibility at ambient pressure. The experimental procedure[5] is just the reverse: accurate data at 1 atm are corrected at three pressures to constant b in order to estimate the solid line in Fig. 5. An assumed linear $t(T)$ also implies increased t and J/t below 100 K, with a 14% decrease in $\chi(0)$, but the phase transition at 54 K requires a model with modulated rather than uniform spacing.

The TTF-TCNQ fit in Fig. 5 captures the temperature dependence of $\chi(T)$. It is not quantitative, however, in view of the difficulty of constant-volume measurements, the limitations to finite N seen in Figs. 2 and 3, and the approximation of linear $t(T)$. Moreover, we have used the same 1D t-J model for electrons on the TCNQ stack and holes on the TTF stack, and we have not considered Coulomb interactions either within or between stacks. The fit is not unique. Small compensating changes in t and J/t lead to closely similar curves. As seen from the constant b data[5] and the present fit, at least half of the observed $\chi(T)$ increase between 100 and 400 K is due to thermal expansion. Orbital contributions account for most of the rest. Our $\chi(T)$ analysis supports the parameter values estimated by Torrance *et al.*[3] The band width of $4t=0.60$ eV at 100 K is typical for π-π stacks in organic conductors, while $U=2t(J/t)=0.86$ eV is indicative of strong correlation.

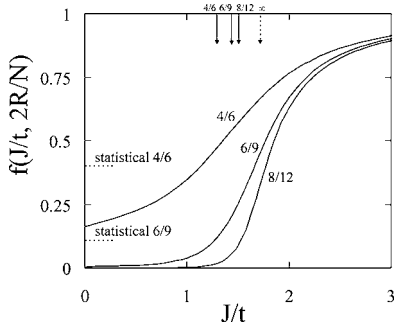

FIG. 6. As a function of J/t, the ground state weight $f_{2R}(J/t,2R/N)$ of having $2R$ adjacent electrons in N-site t-J models at density $\rho=2/3$. Dashed lines are statistical at $J=0$ for 4/6 and 6/9 as discussed in the text. Arrows at $J_c(2R/N)/t>1$ mark crossovers between the variational ground state energy of finite segments and the exact ground state energy of the infinite spin chain. The dashed arrow at $J_c/t=1.72$ is the extrapolated crossover of the infinite chain discussed in the text.

Numerical solutions of finite t-J models contain additional information that bears on the remarkable properties[7–9] of spinless fermions at $J=0$ and on phase separation[11–15] at large J of the GS into regions of filled and empty sites. Virtual transfers in (1) clearly amount to an attractive interaction between singlet-paired spins. Less obviously, the exclusion of two electrons at any site leads to effectively repulsive interactions for real transfers, even though the $J=0$ spectrum is strictly given by the single-particle energies $\varepsilon(r,N)$ in (4). Electron transfer is limited to adjacent occupied and empty sites. Hence, electron configurations with the maximum number of neighboring empty and filled sites are strongly favored at $J=0$. Electrons that are largely kept apart at $J=0$ condense into a single cluster or island at large J.

More quantitatively, we consider sites 1 and N to be neighbors in finite systems with OBC for t and PBC for J. We solve $H(t,J)$, find the GS and compute the weight $f(J/t,2R/N)$ for having $2R$ adjacent electrons in the singlet GS or, alternatively, N-$2R$ adjacent empty sites. Figure 6 shows $f(J/t,2R/N)$ for $\rho=2/3$. Since there are $W(N,2R)$ charge degrees of freedom and N ways to have a single cluster, the statistical probability is $N/W(N,2R)$, or 40% for the 4/6 and 11% for 6/9, as shown by dashed lines. The actual weights are much smaller at $J=0$ and much larger at $J>t$.

The properties of t-J models with larger J are a separate topic.[11–15] The GS of the infinite chain separates with increasing J into regions of filled and empty site. The energy per site in the phase-separated regime is exactly $-2J\rho\ln 2$. To treat small J, we partition the infinite chain into N-site segments with density ρ by deleting t and J in (1) between every Nth neighbor. We find the GS of a segment with specified t and J. The product of GS functions is a trial function for the infinite chain with at most ρN-spin clusters. The variational energy is slightly lower than the segment GS because virtual exchange between sites N and $N+1$ lead to first-order corrections to the energy.[30] The variational energy per site is less than $-2J\rho\ln 2$ for small J. It becomes equal at $J_c(2R/N)$, as shown by arrows in Fig. 6, and is above the spin chain for larger J. The crossovers $J_c(2R/N)$ correspond to phase separation. They extrapolate[30] smoothly to $J_c/t=1.72$ (dotted arrow) for the infinite chain when plotted against $1/N$. Since the infinite cluster is unstable for $J<J_c$, its weight in Fig. 6 is a unit step function at $J_c/t=1.72$.

At $\rho=2/3$, the three variational functions in Refs. 12–14 and the numerical analysis in Ref. 15 all lead to phase separation at $2J/t=3.4-3.5$ within the accuracy of reading graphs, in complete agreement with our result. The variational functions are entirely different approximations for infinite t-J models with arbitrary ρ and parameters that govern attraction or repulsion between fermions. The most elaborate trial function[14] focuses on the spin-gap state at small ρ and on regions of attractive and repulsive Tomonaga-Luttinger liquids. The numerical analysis[15] of phase separation is based on compressibility, which is found as the curvature of the GS energy with respect to N of N-site t-J models with PBC. Although phase separation at $\rho=2/3$ is not demanding, the consistency of Fig. 6 with other approaches is another check of our finite-size treatment.

IV. DISCUSSION

As noted in the Introduction, the spin susceptibility $\chi(0,\rho)$ at $T=0$ of partly filled Hubbard models is proportional to $1/J(\rho)$ to leading order in t/U. Orbital enhancement of $\chi(T,\rho)$ for $U>4t$ can be extracted from previous studies,[19–21] but was not pursued. Since an effective Hamiltonian for virtual exchange in the orbital GS leads[9] to an HAF chain with $J(\rho)$, the first question to consider is why the calculated $\chi(T,\rho)$ of t-J models with $U>4t$ in Figs. 2–5 deviates from HAF chains with the same $\chi(0)$. The reason is that orbital degrees of freedom provide many additional thermally accessible states around $k_BT\sim J(\rho)$.

The simple system of four electrons and six sites is sufficient to illustrate the general case. There are 15 orbital states and the $r=1-4$ levels in (4) are filled in the atomic limit. The $2^4=16$ spin states comprise one quintet, three triplets, and two singlets. Figure 7 shows the lowest four orbital states at $J=0$. For the general case, the smallest orbital gap is the excitation from $r=2R$ to $2R+1$, which according to (4) is

$$E_1(2R,N)=4t\sin\left[\frac{\pi(2R+1/2)}{N+1}\right]\sin\left[\frac{\pi}{2(N+1)}\right]. \quad (14)$$

As expected, E_1 decreases as $1/N$ at constant $\rho=2R/N$. The small gap between E_2 and E_3 is a general result, and $\rho=1/2$ systems with $2R$ electrons have $E_2=E_3$ by symmetry.

The evolution of the PBC spectrum with increasing J/t is shown in Fig. 7. Virtual transfers J split the spin degeneracy. The $S=2$ state (dotted line) of parallel spins is not shifted in this case, while the $S=1$ states (dashed lines) and $S=0$ states (solid lines) are stabilized. The GS orbital spectrum is accurately given by four spins with PBC, whose simple spectrum has singlets at $-2J$, $-6J$ and triplets at $-2J$, $-2J$, $-4J$. The degeneracy and energy differences in E_0 are immediately apparent in Fig. 7. Similar patterns are discernible in E_1, E_2, or E_3 for $J<0.05t$, but deviations appear with increasing J and there is extensive mixing of states by $J=t/4$. For simplicity, we have omitted triplets and singlets that are derived

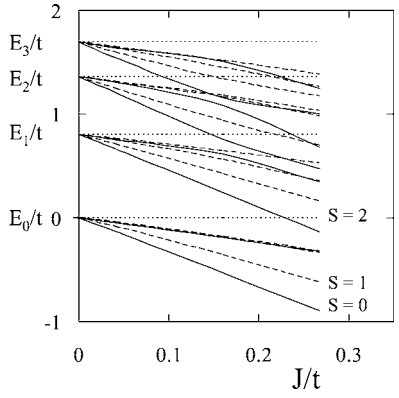

FIG. 7. Evolution with increasing J/t of the low-energy t-J spectrum for four electrons on six sites. The atomic limit ($J=0$) given by Eq. (4) has 16-fold spin degeneracy for each level. Solid, dashed, and dotted lines represent $S=0$, 1, and 2, respectively. The spin energies derived from E_0 are given by a Heisenberg antiferromagnet, as discussed in the text. Spin energies of E_1, E_2, and E_3 show deviations from HAF behavior and mixing with increasing J/t.

from orbital energies greater than E_3, but Fig. 7 includes mixing with such states. The full density of states increases with energy. Although the GS manifold is fully consistent with the Klein-Seitz analysis,[9] deviations from HAF behavior are certain with increasing T as more excited states become thermally accessible.

Orbital mixing increases sharply with N in systems with $\rho<1$ because the excitation energy (14) goes as $1/N$ while the stabilization of spin states increases as ρN. For example, the $\rho=8/12$ version of Fig. 7 has almost half as large E_1 at $J=0$ and 64 spin states for each orbital energy. Remarkably, Shiba's exact[10] $\chi(0,\rho)$ for the infinite Hubbard model matches to leading order in t/U the Klein-Seitz[9] effective $J(\rho)$. For any finite T, however, orbital contributions in systems with $\rho<1$ increase $\chi(T)$ compared to an HAF. Orbital contributions increase with decreasing density in Fig. 4 and roughly double the maximum spin susceptibility at $\rho=1/2$.

We noted in connection with $\chi(T)$ in Fig. 5 the difficulties of comparing experiment and theory in systems with substantial thermal expansion. In contrast to evidence for orbital contributions to the susceptibility, the $\chi(T)$ analysis of TTF-TCNQ is approximate. Quite aside from interchain interactions whose role has been discussed in both conjugated polymers and organic solids with stacked structures, Coulomb interactions between sites cannot be neglected in partly filled bands. A nearest-neighbor interaction V along the stack leads to an extended Hubbard model, while long-range Coulomb interactions correspond to a Pariser-Parr-Pople model.

Finite $V>0$ is an explicit repulsion between electrons on adjacent sites. The generalization of the t-J model (1) to finite V does not increase the difficulty of numerical solutions. It adds an extra parameter, however, and spoils the connection to the exact $\chi(0)$ of Hubbard models with $U>4t$ that we have exploited above. At fixed t and $J<t/2$, we find $\chi(T)$ to increase systematically with $V/t=1,2$, and 4 for all ρ in Figs. 2–5. The modest increase for $V/t=1$, for example, yields alternative 6/10 fits for the TTF-TCNQ susceptibility with slightly different t and J. We interpret the small increase with V as another indication that t already keeps the electrons apart when $n_p=2$ sites are excluded and J is small. The AF exchange constant J also depends on V through the energy of the virtual singlet state, which is U-V at $\rho=1$. Such dependence is difficult to identify in the t-J model, however, since t and J are independent parameters.

Although the intense scrutiny of TTF-TCNQ has abated, it remains a prototypical organic conductor of current interest.[2,31,32] The TTF and TCNQ stacks have characteristic transitions at low temperature. Hubbard or extended Hubbard models with different parameters for each stack are likely. Indeed, photoelectron data of the surface has been interpreted[32] in terms of small U for one stack, large U for the other. Similar $\chi(T)$ is inferred above 60 K in crystals from the average g-tensor of the exchange-narrowed electron paramagnetic resonance line,[33] but different $\chi(T)$ and bandwidths are inferred from ^{13}C NMR spectra.[34] We have not differentiated between TTF and TCNQ stacks aside from checking that similar t-J parameters in two models lead to similar total $\chi(T)$ curves.

The proper extended Hubbard model and its parameter values are still open for TTF-TCNQ. It is plausible in $\rho<1$ systems to associate transport as usual with t in partly filled bands and magnetism with strong correlation $U>4t$. Such a comprehensive analysis of magnetism, transport, and other properties is not yet available. Conversely, now that the $\chi(T)$ fit in Fig. 5 has been obtained with parameters in the range suggested by Torrance *et al.*,[3] a comparably good fit must be produced by small U models. More generally, direct solution of finite systems is a promising approach to the susceptibility of extended 1D systems with low-energy spin excitations. We have shown that equal $\chi(0,\rho)$ per electron given by $J(\rho)$ in (2) lead to different $\chi(T,\rho)$ around $k_BT\sim J(\rho)$ for $\rho<1$. Hence the spin susceptibility of partly filled bands with $U>4t$ cannot be modeled by a Heisenberg AF or a Hubbard model with $\rho=1$.

ACKNOWLEDGMENT

We thank the Princeton Institute on the Science and Technology of Materials (PRISM) for partial support of this work.

[1] *Chemistry and Physics of One-Dimensional Metals*, edited by H. Keller, NATO ASI Series B25 (Plenum, New York, 1977), and references therein.
[2] D. Jerome, Chem. Rev. (Washington, D.C.) **104**, 5565 (2004), and references therein.
[3] J. B. Torrance, Y. Tomkiewicz, and B. D. Silverman, Phys. Rev. B **15**, 4738 (1977); a polynomial expression for $\chi(T)$ the HAF chain is given in Ref. 60; J. B. Torrance in Ref. 1.
[4] J. E. Gulley and J. F. Weiher, Phys. Rev. Lett. **34**, 1061 (1974); J. C. Scott, A. F. Garito, and A. J. Heeger, Phys. Rev. B **10**, 3131 (1974).
[5] S. Klotz, J. S. Schilling, M. Weger, and K. Bechgaard, Phys. Rev. B **38**, 5878 (1988).
[6] F. C. Zhang and T. M. Rice, Phys. Rev. B **37**, 3759 (1988).
[7] E. Lieb and D. Mattis, Phys. Rev. **125**, 164 (1962).
[8] W. F. Brinkman and T. M. Rice, Phys. Rev. B **2**, 1324 (1970).
[9] D. J. Klein and W. A. Seitz, Phys. Rev. B **20**, 3217 (1979).
[10] H. Shiba, Phys. Rev. B **6**, 930 (1972).
[11] J. Sirker and A. Klumper, Phys. Rev. B **66**, 245102 (2002).
[12] C. S. Hellberg and E. J. Mele, Phys. Rev. Lett. **67**, 2080 (1991).
[13] H. Yokoyama and M. Ogata, Phys. Rev. B **53**, 5758 (1996).
[14] K. Kobayashi, C. Ohe, and K. Iguchi, Phys. Rev. B **54**, 13129 (1996).
[15] M. Ogata, M. U. Luchini, S. Sorella, and F. F. Assaad, Phys. Rev. Lett. **66**, 2388 (1991).
[16] M. Takahashi, Prog. Theor. Phys. **47**, 69 (1972).
[17] Z. N. C. Ha, Phys. Rev. B **46**, 12205 (1992).
[18] M. Takahashi and M. Shiroishi, Phys. Rev. B **65**, 165104 (2002).
[19] T. Usuki, N. Kawakami, and A. Okidi, J. Phys. Soc. Jpn. **59**, 1357 (1990).
[20] G. Jüttner, A. Klümper, and J. Suzuki, Nucl. Phys. B **522**, 471 (1998).
[21] J. E. Hirsch and D. J. Scalapino, Phys. Rev. B **27**, 7169 (1983).
[22] J. C. Bonner and M. E. Fisher, Phys. Rev. **135**, A640 (1964).
[23] Z. G. Soos and S. A. Bewick, Chem. Phys. Lett. **421**, 210 (2006).
[24] D. C. Johnston, R. K. Kremer, M. Troyer, X. Wang, A. Klumper, S. L. Bud'ko, A. F. Panchula, and P. C. Canfield, Phys. Rev. B **61**, 9558 (2000), and references therein.
[25] S. Ramasesha and Z. G. Soos, in *Theoretical and Computational Chemistry*, Vol. 10, edited by D. L. Cooper (Elsevier, Amsterdam, 2002), p. 635.
[26] Z. G. Soos and S. Ramasesha, in *Valence Bond Theory and Chemical Structure*, edited by D. J. Klein and N. Trinajstic (Elsevier, Amsterdam, 1989), p. 81.
[27] S. Eggert, I. Affleck, and M. Takahashi, Phys. Rev. Lett. **73**, 332 (1994).
[28] A. J. Schultz, G. D. Stucky, R. H. Blessing, and A. J. Coppens, J. Am. Chem. Soc. **98**, 3194 (1976).
[29] E. M. Conwell, Phys. Rev. B **22**, 1761 (1980).
[30] S. A. Bewick, Ph.D. thesis, Princeton University, 2006.
[31] M. Sing, U. Schwingenschlogl, R. Claessen, P. Blaha, J. M. P. Carmelo, L. M. Martelo, P. D. Sacramento, M. Dressel, and C. S. Jacobsen, Phys. Rev. B **68**, 125111 (2003).
[32] R. Claessen, M. Sing, U. Schwingenschlogl, and J. M. P. Carmelo, J. Phys. IV **114**, 51 (2004).
[33] Y. Tomkiewicz, A. R. Taranko, and J. B. Torrance, Phys. Rev. Lett. **36**, 751 (1976).
[34] T. Takahashi, D. Jerome, F. Masin, J. M. Fabre, and L. Giral, J. Phys. C **7**, 3777 (1984).